Deposition of Sodium Sulfate in a Heated Flow of Supercritical Water

Steven N. Rogak and Paul Teshima
Dept. of Mechanical Engineering, University of British Columbia, Vancouver, BC, V6T 1Z4 Canada

Wastes that can be treated by supercritical water oxidation often contain salts. Salts are almost insoluble under supercritical conditions and can result in severe fouling. A simple heat- and mass-transfer model was developed and tested experimentally for sodium sulfate in a fully turbulent flow of water at 25 MPa. This model uses empirical heat-transfer correlations to estimate mass-transfer rates. The diffusion coefficient of the salt is calculated from the Stokes-Einstein relation using a hydrodynamic diameter of 2 to 6 Å. New measurements of solubility showed that the solubility of sodium sulfate decreases by a factor of about 1,000 as the temperature increases from 380°C to 400°C. Salt deposition rates, inferred from the outside temperature of a heated test section, were reasonably close to the model predictions.

Introduction

Supercritical water oxidation technology

Supercritical fluids are finding increasing industrial use, largely because of their ''tunable" solvation properties (Hutchenson and Foster, 1995). Supercritical water is a particularly important fluid because of its involvement in geochemistry and steam power systems. The IAPWS conferences (White et al., 1995) review a broad range of scientific work conducted on supercritical water. The present work was motivated by a relatively new technology, supercritical water oxidation.

Water above its critical point (374°C and 22.1 MPa) is an excellent solvent for organic compounds and gases (including oxygen). Thus, supercritical water oxidation (SCWO) of organic wastes can take place without interphase mass-transfer resistance. In the last two decades, there has been considerable progress in understanding reaction kinetics in supercritical water, corrosion of reactor walls and other practical issues. Shaw et al. (1991), Tester et al. (1993), and Gloyna and Lixiang (1995) provide reviews of supercritical water oxidation. Compared with other waste treatment techniques, SCWO will probably be most competitive for very wet, pumpable organic wastes that are particularly toxic or are not treatable by biological methods.

Correspondence concerning this article should be addressed to S. N. Rogak.

Salt deposition in supercritical water

It was recognized very early in SCWO development that while organics are miscible in supercritical water, inorganic salts are not. This reversal of water's normal character means that wastes containing salt or salt precursors can cause severe fouling in SCWO systems. The amount and type of salt varies with the waste source. Pulp mills create numerous streams with sulfate, carbonate, and chloride concentrations up to 0.1 wt. % (Cooper et al., 1997; Goldacker et al., 1996). Military marker dyes and flares contain large amounts of sodium sulfate and other inorganics up to several percent by weight (Rice et al., 1994). In some cases, wastes might contain several wt. % sodium hydroxide, which is expected to precipitate in supercritical water or result in the formation of other salts (Buelow et al., 1993). Chlorinated wastes can produce hydrochloric acid, which is soluble, but will react with any base in the system to produce salts.

Fouling concerns have led to the development of several reactors designed specifically to prevent fouling from salts. These designs fall into two distinct classes. The transpiring wall systems use clean water and a porous inner reactor liner to maintain a barrier between the reactor wall and the salty flow. The MODAR-type system uses a large-diameter vessel with salty reactants flowing down the center of the vessel into a salt settling chamber, and salt-free products flowing up along the wall of the vessel. Even this design is not entirely

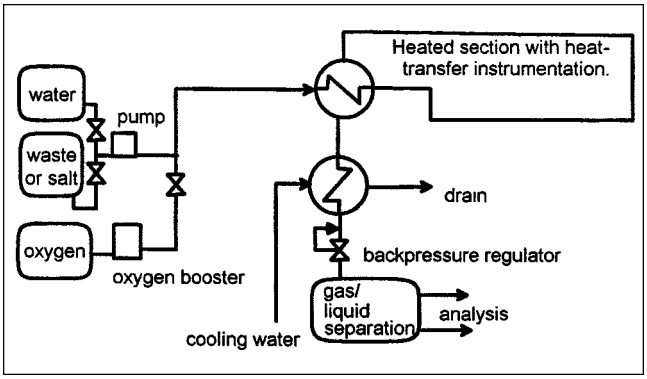

Figure 1. SCWO pilot plant.

For salt deposition experiments, the oxygen and waste feed systems are disconnected.

free from fouling, as suggested by the salt particle trajectories computed by Oh et al. (1997). While such systems may be needed in extremely salty wastes, a long, plug-flow tubular reactor is easier to control and design. It should be noted that the commercial Huntsman system in Texas uses a long tubular reactor (McBrayer and Griffith, 1996). If fouling cannot be prevented completely, one must be able to predict how quickly a reactor can be plugged.

Although fouling will clearly be influenced by the complex mixtures in a SCWO system, we have chosen to study a binary salt-water mixture for the first stages of model development and validation. In the present work we examine fouling in supercritical water using experiments and modeling. The pilot plant used here is shown in Figure 1. The reactor is of the simple tubular type, which facilitates interpretation of experiments. Sodium sulfate was investigated, because it is common, has a simple phase diagram for the conditions in our facility, and because there have been some earlier studies on this salt.

Modeling Salt Deposition

Salt deposition kinetics depend on whether or not particles of salt form in the bulk fluid. If a salt solution in a heated tube is rapidly taken above the critical temperature, a supersaturated solution may result. The supersaturation will be reduced by either nucleation of salt particles, or diffusion of salt molecules to the hot walls. Particulate salt, depending on particle size and flow Reynolds number, may be transferred to the wall at a greater or lesser rate than individual salt molecules. According to homogeneous nucleation theory, whether or not particles form depends on the superaturation of the solution, the particle surface tension, and diffusional parameters. Armellini (1993) and Hodes et al. (1997) have examined some aspects of Na_2SO_4 nucleation in supercritical and near-critical water, but so far there have been no results published for supercritical water in a heated tube and the fundamental data needed to model the nucleation are not known. In the experiments discussed later, it appears that the bulk solution never becomes supersaturated, so nucleation is not modeled here.

A second simplification is the use of pure-water thermodynamic properties (Pruss and Wagner, 1995) and transport properties (Haar et al., 1984) to model the solution. Hodes (1998) has used work from NIST to model subcritical solutions of sodium sulfate. For the conditions in the present work, the density of the salt solution might be 5% to 15% higher than that of pure water and the thermal diffusivity would be changed somewhat less. The uncertainties in the turbulent heat- and mass-transfer correlations used here are probably larger than these effects. We have therefore avoided the difficult (and uncertain) task of modeling the effect of salt on transport properties.

We are concerned with fully turbulent flows of supercritical water carrying traces of salt. The fluid core is assumed to be well mixed from the point of view of temperature and concentration gradients, but there are finite heat- and mass-transfer coefficients at the wall. The essential problem is to determine the wall and bulk temperatures (T_w, T_b) and the bulk salt mass fraction X_b (see Figure 2). This approach differs somewhat from the work of Chan et al. (1994), in which heat- and mass-transfer resistances were neglected. Although their model was applied successfully to sodium sulfate in a small ($\sim$ 0.036 kg/min) supercritical water system, there are several reasons why this model cannot be used in all cases. Firstly, since $T_w > T_b$, salt deposition should start before $X_{\text{sat}}(T_b) = X_b$. Secondly, the mass-transfer rate for salt molecules may be slow for particular conditions. We consider these effects explicitly in the present work.

Heat- and mass-transfer relations are developed for a turbulent flow of water at mass-flow rate $\dot{m}$ in a tube of radius r. The water enters some specified portion of the tube with concentration X_b of dissolved salt. The heat flux per unit area is q. An enthalpy balance over a length dz of tubing yields the change in bulk fluid temperature T_b

$$\frac{dT_b}{dz} = \frac{2\pi rq}{\dot{m}c_p(T_b)} \tag{1}$$

where the specific heat c_p is a strong function of temperature near the critical point. The wall temperature T_w is determined by the heat-transfer coefficient h according to

$$T_w = T_b + \frac{q}{h} \tag{2}$$

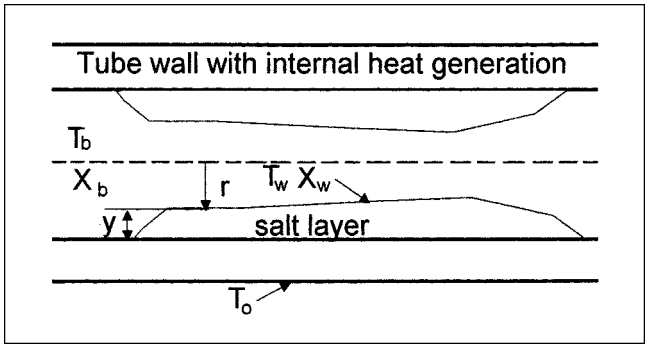

Figure 2. Notation used to describe simultaneous heat and mass transfer to a section of tube with inside radius *r*.

We have used the heat-transfer correlation developed by Swenson et al. (1965) for pure water near the critical point

$$Nu = \frac{2hr}{k_w} = 0.00459 \left(\frac{2Gr}{\mu_w} \right)^{0.923} \left(\frac{H_w - H_b}{T_w - T_b} \frac{\mu_w}{k_w} \right)^{0.613} \left(\frac{\rho_w}{\rho_b} \right)^{0.231} \tag{3}$$

In this correlation k, μ, and ρ are the fluid conductivity, viscosity and density, respectively; G is the mass-flow per unit cross-sectional area, and H is the enthalpy. Thus, the first term is Reynolds number and the second term is a Prandtl number in which the effective heat capacity is calculated from the difference between the bulk and wall enthalpies. In the experimental system, heating is provided by passing electrical current through the tube walls. We measure the outer temperature rather than the inside wall temperature and have therefore modeled the radial heat conduction through the tube walls to obtain the outer temperature of the tube T_o. We assume uniform heat generation, constant thermal conductivity in the tube wall, and radial symmetry. In experiments with clean water, predicted and measured temperatures differed by less than 3°C typically, compared with values of $T_o - T_b$ of up to 30°C. Buoyancy and entrance-length effects were not expected or observed for our experimental conditions.

The maximum dissolved salt weight fraction $X_{\text{sat}}(T)$ decreases as T increases above the critical temperature. When the temperature in a heated flow reaches the point where $X_{\text{sat}}(T) < X_0$, then we expect a new salt phase to form. For sodium sulfate, the new phase is solid salt (Armellini and Tester, 1993; Franck, 1971). In a heated tube, the solution first becomes saturated at the wall. Once deposition has started, if there is no attachment resistance, the solid salt will simply be in equilibrium with the solution at the wall

$$X_w = X_{\text{sat}}(T_w) \tag{4}$$

In general, there is a concentration difference between the wall and bulk leading to a mass flux q_m to the wall

$$q_m = \rho V_D (X_b - X_w) \tag{5}$$

where ρ is taken as the bulk fluid density and V_D is the deposition velocity or mass-transfer coefficient. Lacking data on mass transfer, V_D is estimated from Eq. 3, but with thermal conductivity replaced by molecular diffusivity D, and the Prandtl number replaced by the Schmidt number ($\mu/\rho D$)

$$\frac{2V_D r}{D_w} = 0.00459 \left(\frac{2Gr}{\mu_w} \right)^{0.923} \left(\frac{\mu_w}{\rho_w D_w} \right)^{0.613} \left(\frac{\rho_w}{\rho_b} \right)^{0.231} \tag{6}$$

The diffusivity is calculated from the Stokes-Einstein relation

$$D = \frac{k_B T}{3\pi\mu d_H} \tag{7}$$

where k_B is the Boltzmann constant and d_H is the effective hydrodynamic diameter. This diameter is difficult to estimate because the degree of ion association and hydration is not known for sodium sulfate in near-critical water. For modeling, we will choose a range of diameters based on indirect evidence. Hodes et al. (1997) measured sodium sulfate deposition rates in slightly subcritical water. These measurements were consistent with a hydrodynamic diameter of about 2 Å. In comparison, the molecular diameter of solid sodium sulfate (based on density and molecular weight) is about 5.5 Å. Butenhoff et al. (1996) measured the diffusion coefficient of sodium nitrate in supercritical water. Far from the phase separation pressure and temperature, the hydrodynamic diameter was 6 to 7 Å. This is roughly consistent with a sodium nitrate ion pair with four associated water molecules. Near phase separation, ''critical slowing'' resulted in much lower diffusivities, equivalent to diameters of 60–70 Å. Protopopov et al. (1994) modeled the diffusion of iron corrosion products, including a correction for critical slowing. Their correction at 25 MPa was a factor of 11 reduction near the pseudocritical temperature. Below 380°C and above 390°C, the correction factor was not significant. Mass-transfer modeling is further complicated by the possibility of significant thermal diffusion (Soret effect) near the critical point (Butenhoff et al., 1996). This effect would reduce the mass transfer of salt to a heated wall.

Considering this previous work, it is conceivable that the effective hydrodynamic diameter of sodium sulfate varies from 2 to 60 Å as the fluid temperature rises past the critical temperature. The functional form of this variation is difficult to model, so we perform model calculations for three diameters: 2, 6 and 60 Å.

The mass-transfer and bulk salt concentration are linked by conservation of mass

$$\frac{dX_b}{dz} = -\frac{2\pi r q_m}{\dot{m}} \tag{8}$$

Equations 1-8 can be integrated numerically. The thickness of the deposit is then obtained by integration of the flux over time. The effective salt layer density is related to the porosity of the layer. We have chosen a porosity of $\phi = 0.71$ based on Hodes et al. (1997). This parameter has a strong influence on the modeled thickness, but will not affect the comparisons with the measured salt profiles, because the same value of porosity is used in the analysis of the experimental data.

Examples of predicted salt thicknesses are shown in Figure 3. The experimental conditions are described in Table 1. Several features of the model thicknesses are worth noting. Chan's model (very fast heat and mass transfer) always predicts that the salt is deposited over a relatively short distance along the tube. Deposition is delayed until the *bulk* solubility is exceeded, rather than beginning as soon as the solubility at the *wall* is exceeded. Comparisons of the models with measurements will be discussed below.

Experimental Studies

Experimental facility

The UBC/NORAM pilot plant is shown in Figure 1. Water with or without Na_2SO_4 is pumped by a triplex plunger pump (0.6 to 2 L/min flow rate range) through a rengenera-

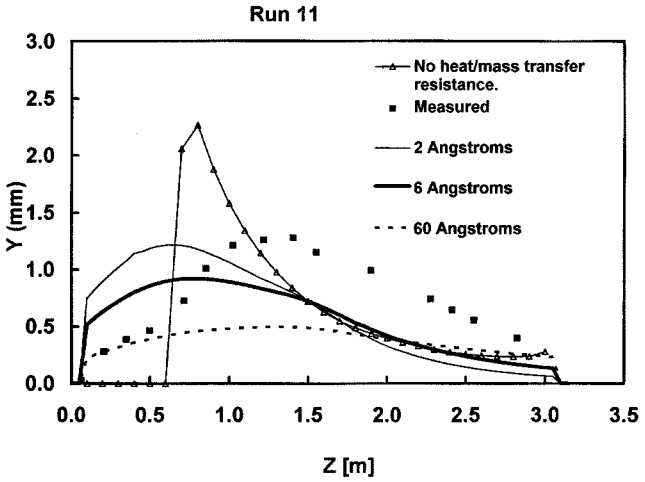

Figure 3. The present model is compared to Chan et al.'s model (1994), which neglects heat- and mass-transfer resistance.

The conditions for Run 11 are given in Table 1.

tive heat exchanger, two electric preheaters, and finally the test section. Pressure is controlled by a backpressure regulator downstream of the process cooler. All experiments were conducted near 25 MPa.

The test section is formed from two 1.6 m lengths of Inconel 625 nickel alloy tubes (6 mm ID). The test section includes arrangements for measuring bulk fluid temperature at 5 points and outside wall temperature at approximately 16 points along the upper surface. Electrical current passes through the walls of the preheaters and test section. Power was estimated from bulk temperatures of the flowing water. The test section is insulated with an average of 9 cm of uniform, rigid ceramic fiber insulation.

Table 1. Summary of Salt Deposition Experiments*

Run. No.	Inlet Conc. (wt. %)	Mass Flow (kg/min)	Heat Flux (kW/m)	$T_{b,\text{in}}$ (°C)	$T_{b,\text{out}}$ (°C)	Pres. (MPa)	Run Time (s)	k (W/m·K)
1	0.652	1.21	2.07	373	384	24.7	183	
2	0.652	0.66	0.81	375	384	25.2	336	
3	0.595	1.2	2.04	373	384	24.7	203	
4	0.595	2.22	2.68	372	384	25.4	110	
5	0.595	0.68	1.17	371	386	25.5	358	
6	0.58	1.21					206	
7	0.58	2.21					113	
8	0.58	0.64					390	
9	0.408	0.62	1.52	371	388	25.4	574	
10	0.408	1.23	2.98	363	386	25.3	289	
11	1.066	2.16	5.58	365	386	25.1	63	
12	1.066	0.7	1.81	364	386	25.1	193	
13	0.195	2.18	5.73	363	386	25.1	342	
14	0.195	0.63	1.66	365	388	25.8	1,184	
9a	0.408						620	2.5
10a	0.408						510	9.4
11a	1.066						80	5.2
12a	1.066						478	9.8
13a	0.195						342	4.1
14a	0.195						1,890	3.7

Profiles for runs 9–14 are plotted for the times given here. Conductivity was determined from the same experiments, but using a longer time for mass collection (Run No. 9–14a).

Solubility experiments

Measurements of solubility of sodium sulfate near 250 bar and slightly subcritical temperatures have been made by Ravich and Borovaya (1964), Armellini and Tester (1993), Hodes (1997), and DiPippo (1998). Shvedov and Tremaine (1997) made additional measurements and developed a correlation for mole fraction x

$$\ln(x) = -10.47 - 27{,}550/T + (4{,}805/T)\ln\rho \qquad (9)$$

where ρ is the water density (kg/m^3) at the specified temperature T (K). This correlation appears to underestimate solubility by up to 20%, compared with the other measurements. At supercritical temperatures, the discrepancies are far greater. At 250 bar and 500°C, Armellini and Tester (1993) measured a solubility of about 1 ppm (by weight). Measurements by Morey and Hesselgesser (1951) at 500°C, 133 bar, and 500°C 666 bar can be interpolated to give a solubility of about 80 ppm. Interpolation of solubilities given by Martynova (1976) (500°C, 300 bar) and Martynova and Samoilov (1962) (500°C, 200 bar) suggests a solubility of about 0.4 ppm.

Our own solubility measurements for Na_2SO_4 are summarized in Table 2 and Figure 4. The most striking result is the rapid decrease in solubility just above the pseudocritical temperature. (For pressures above the critical pressure, the pseudocritical temperature marks the maximum compressibility. This is nearly the same temperature at which specific heat is maximum, which is 385°C at $P = 25$ MPa.) We have used a procedure based on the work of Chan et al. (1994). The salt solution is pumped through the heated reactor and sampled at the end. As the solution is heated, salt will deposit on the

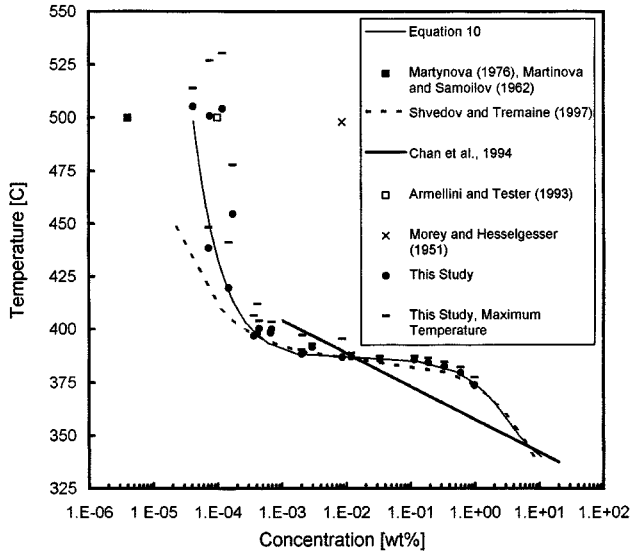

Figure 4. Comparison of sodium sulfate solubility measurements at 25 MPa.

Table 2. Sodium Sulfate Solubility Measurements at 25 MPa*

File	Feed Conc.	Avg. Temp.	Max. Temp. Modeled	Effluent Conc.	
	(ppm)	(°C)	(°C)	(ppm)	
may30a	621	396.9	406.5	3.66	
may30b	621	398.4	399	6.65	+
may30c	621	388.5	390.3	20.2	
may30d	621	391.6	393.2	29.5	+
may30e	621	387.2	388.8	119	
may30f	621	385.9	387.3	335	
may30g	621	385.8	387.3	1,150	
jun27a	11,400	379.7	382.2	6,000	
jun27b	11,400	373.9	377.6	9,900	
jul3a	6,210	384.5	386.6	1,900	
jul3b	6,210	382.7	384.6	3,360	
jul21a	685	454.6	477.9	1.74	
jul21b	685	397.9	412	4.14	
jul22	4.84	419.6	441.3	1.48	
jul23a	4.84	500.9	527	0.76	
jul23b	4.84	504.3	530.5	1.19	
jul28	696	438.6	448.4	0.72	+
aug8	532	505.3	513.9	0.42	+
aug26a	194	400.4	404.1	4.42	b
aug26b	194	400	403.6	6.91	
aug26c	194	388.8	397.3	20.8	b
aug26d	194	387	395.5	86.1	

*All experiments were conducted at a flow of 1.2 kg/min, except those marked with + (0.65 kg/min). Two experiments (marked b) were dissolution (''salt bed'') rather than deposition experiments.

walls because the solubility decreases with temperature. If mass transfer is sufficiently rapid, the effluent concentration will be at the solubility limit of the hottest part of the reactor. Chan et al. assumed that the bulk fluid temperature of their isothermal test section controlled the concentration of salt in their effluent. They measured solubility at four temperatures (three subcritical and one supercritical) and found that the results were well represented by the straight line shown in Figure 4. (Data in Chan et al. (1994) are reported as wt. %, but the numbers are actually wt. fraction, based on the presentation of the same data in LaJeunesse and Rice (1994).) In the present study, we assumed the average bulk temperature of our nearly isothermal test section controlled the effluent salt concentration. This assumption will be discussed below. Two flow rates (0.65 and 1.2 kg/min) were used. A few experiments were performed using a modified procedure, labeled ''salt-bed'' in Table 2. In this procedure, clean water was fed into a previously-fouled test section. It was thought that the mass-transfer kinetics might alter the apparent solubility, but there is no consistent variation caused by flow rate or experiment configuration.

Our measurements are close to Eq. 9 for $T < 400$°C, and close to the Armellini and Tester (1993) measurement at 500°C. Given the appearant scatter in the measurements, a discussion of experimental uncertainities is warranted.

We calibrated our type-K Inconel-sheathed thermocouples (Omega) at 0°C and 100°C. Based on the manufacturer's data for the thermocouples and the data acquisition system (Omega Multiscan 1200), the accuracy and repeatability should have been better than 1°C. Prior to performing the salt deposition experiments, we confirmed available heat-transfer correlations for near-critical water. The results of that comparison suggest that the overall, absolute temperature error is less than 5°C. Salt concentration was determined using an Omega CDH-287 conductivity meter. Measurements of the effluent pH confirmed that no hydrolysis took place during the experiment, therefore, the conductivity-concentration relations for the standard solutions would be applicable to the effluent from the SCWO facility. Measurements on solutions of known concentration indicated that the error was less than 10%.

Flow rate was measured periodically using a graduated cylinder and stopwatch, and was always well within 10% of the nominal flow rates given in Figure 4 (see Table 2).

System pressure varied several percent around the nominal value of 25 MPa. This would alter the psuedocritical point by 2 or 3°C. Note that the data by Chan et al. and Armellini are for nominal pressures of 250 atm (25.3 MPa), which is within the uncertainty of our pressure regulation.

Greater uncertainty is introduced by heat- and mass-transfer effects in the system. For the experimental conditions pertaining to each solubility measurement, we modeled the heat transfer in the preheaters and test section. Naturally, the heated walls were at a higher temperature than the bulk fluid at the same axial position, and, in many cases, the preheater walls were much hotter than the bulk fluid temperature leaving the test section. The resulting maximum temperatures were plotted in Figure 4. The true temperature corresponding to a particular solubility should lie between the test-section temperature and this maximum temperature. This introduces an uncertainty of up to 20°C, but only for the high-temperature measurements; the solubility-temperature relation is not changed greatly by this reinterpretation of the temperature measurements.

Mass-transfer modeling (discussed earlier and verified in the experiments discussed below) indicated that the UBC test-section was sufficiently long for salt to deposit on the walls. Heat-and mass-transfer effects might have been important in the experimental facility at Sandia used by Chan et al. That system was not as slender as the UBC system, and probably ran with higher wall-bulk temperature differences during preheating. This might explain why their concentrations at subcritical temperatures are less than expected.

We have fit our solubility measurements to the following relations

$$X_{\text{sat}} = \begin{cases} -3.49612 \ln\left(\dfrac{T - 337.70602}{49.11281}\right) & 337.7 < T < 385.8 \\ 10^{232.3458 - 0.605186T} & 385.8 < T < 388.5 \\ \dfrac{2.2}{32.19(T - 385.645)\ln(1{,}000T^{1.2})} & T > 388.5 \end{cases} \tag{10}$$

Temperature is in °C, and salt concentration X_{sat} is in wt. %. Clearly, a thermodynamically consistent correlation would be needed to extrapolate the results to other pressures, but Eq.

10 is adaquate for the present study which was conducted at one pressure.

Deposition experiments

Fourteen experiments were run to examine the distribution of deposited salt in our test section with constant heat flux per unit length (Table 1). Flow was varied from 0.62 to 2.22 kg/min, which results in fully turbulent flow. For example, 1 kg/min at 380°C and 25 MPa corresponds to a Reynolds number of about 70,000. Because the fluid viscosity decreases as temperature increases, a typical test section inlet Reynolds number is 30,000 while the outlet Reynolds number might be about 200,000. Inlet salt concentration varied from 0.195 to 1.066 wt. %. Inlet temperature was always below the pseudo-critical temperature for 25 MPa, and the outlet temperature was close to the pseudocritical temperature. This is a narrow set of conditions, but includes the temperature range where the greatest fouling can occur. Run times of 1 to 20 min were needed to accumulate sufficient quantities of salt.

Salt thickness was inferred from outside tube temperatures, which could be measured reliably. For example, runs 3, 4, and 5 had the same nominal conditions as runs 6, 7 and 8, respectively, and the fouling-induced temperature changes were reproduced to within 6%. The experimental difficulty lies in determining the effective deposit conductivity, which is needed to model the radial conduction in the salt layer, thereby relating temperature to deposit thickness. The deposit conductivity depends on the deposit porosity (0.71 was used) and the salt conductivity. We have treated the salt and

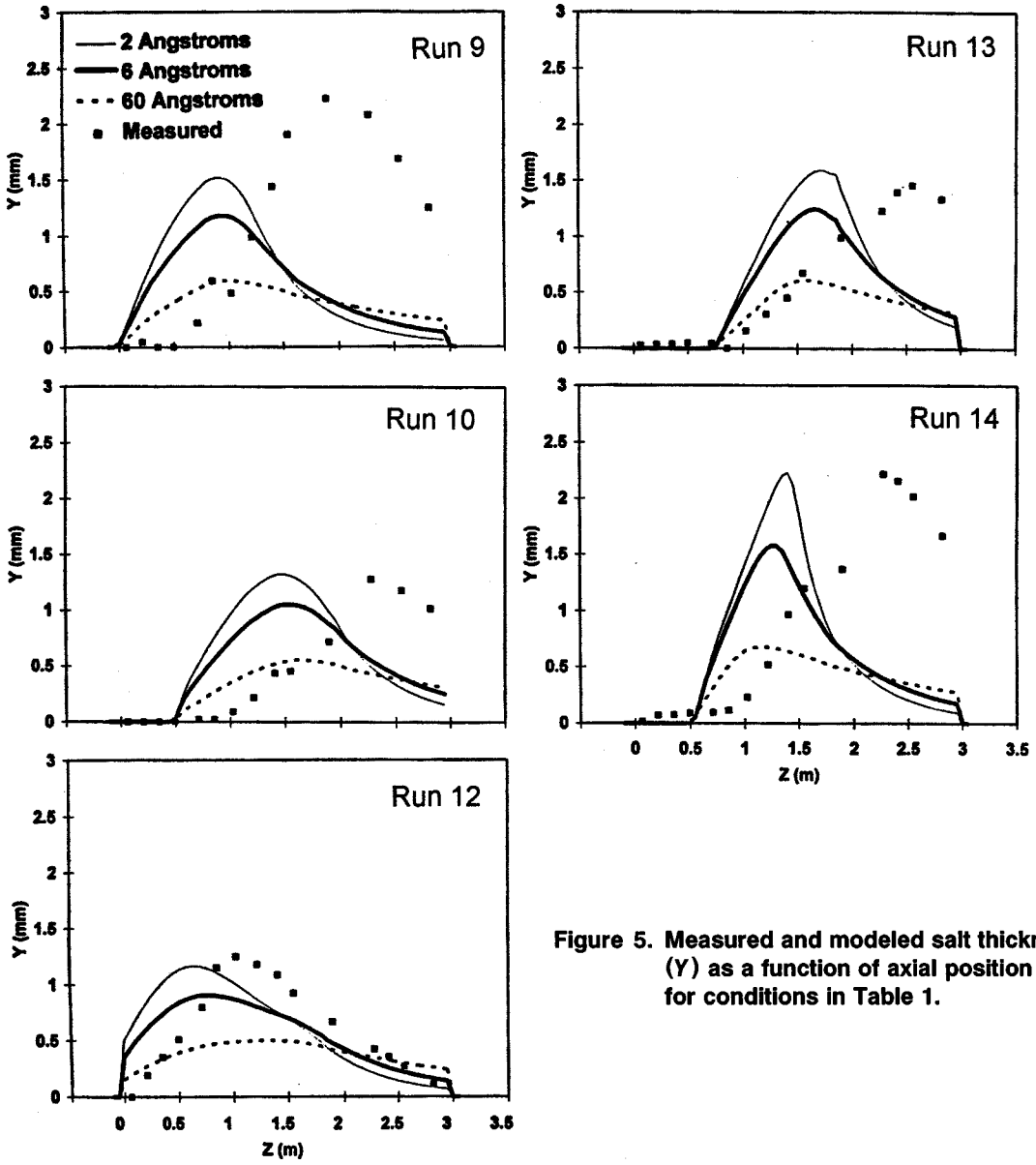

Figure 5. Measured and modeled salt thicknesses (Y) as a function of axial position (Z) for conditions in Table 1.

pore volume as parallel conduction paths. This is not a critical assumption, because the salt conductivity was treated as an adjustable parameter chosen to achieve mass balance, as described below.

By measuring inlet and effluent concentrations during an experiment, we can calculate the mass that should have deposited in the test section. We compare this with the inferred salt thickness (obtained from the temperature measurement) integrated over the tube length and then adjust conductivity to achieve mass balance. This was done for runs 9 to 14 (see lines 9a-14a in Table 1). The run-specific conductivities were averaged, giving an apparent salt conductivity of 5.8 W/m-K. This value was then used for the analysis of all experimental runs. We could not find Na_2SO_4 conductivity measurements for our conditions, but note that the conductivity of NaCl at similar temperatures is between 4 and 5 W/m·K. The inferred salt thicknesses were consistent with differential pressure measurements as well. When inferred thicknesses increased above 2 mm (tube radius = 3 mm), pressure drop measurements indicated that the tube was close to plugging. Thus, our fitting constants are physically plausible.

Comparison of Model with Experimental Results

When we first compared the measured and predicted peak salt thicknesses, discrepancies were on the order of a factor of 2 to 3, and there appeared to be qualitatively different behavior for the last runs performed. One difference with the last runs (9 to 14) is that the inlet bulk temperature is well below the psuedocritical temperature, where solubility is high. We believe that in the earlier runs, the preheater walls were sufficiently hot to cause salt deposition before the test section. For this reason, we did not perform mass balances for these runs. Deposit conductivities were inferred from experiments in which all the salt was known to be deposited in the test section.

Figures 3 and 5 compare measured and modeled deposit distributions for all experiments free from preheater deposition. Three model curves are presented in each case, corresponding to salt hydrodynamic diameters d_H of 2, 6 and 60 Å. Compared to the modeled peak, the measured peak is high, and delayed. There are several possible explanations of this discrepancy. First, it is possible that the heat- and mass-transfer rates are higher than predicted. Higher heat-transfer coefficients result in a cooler tube wall, which delays the deposition. The magnitude of the temperature discrepancy corresponding to the delayed peak is only about 3°C, as can be seen for Run 11 (Figure 6). A combination of measurement error, roughness-enhanced transport, and flow development effects (due to the acceleration of the fluid as it is heated) might account for the shift. The curves might also be shifted by rapid changes in the salt diffusivity near the critical point, but it is impossible to resolve such features in the current experimental results.

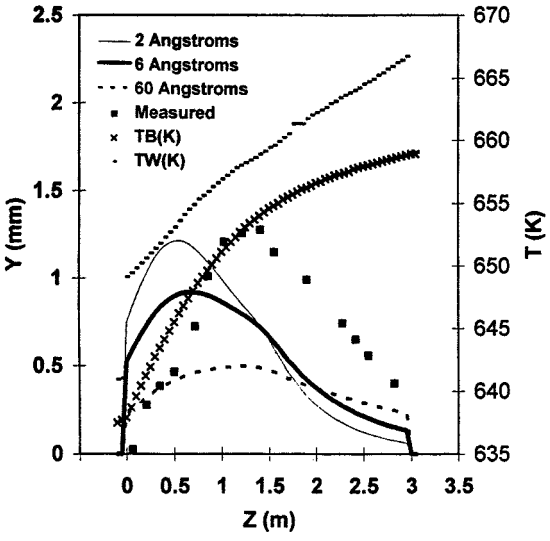

Figure 6. Superposition of wall (TW) and bulk (TB) fluid temperatures over the salt thickness profiles.

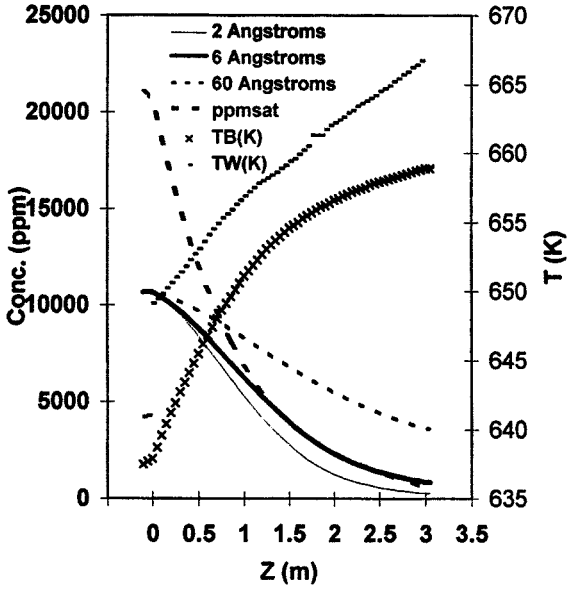

Figure 7. Bulk fluid concentration predicted for three salt hydrodynamic diameters as a function of axial position, compared with solubility limit (" ppmsat") and the wall and bulk temperatures.

The salt deposition model does not include particle nucleation, and as shown in Figure 7, the bulk salt concentration remains below the solubility limit for $d_H = 2$ and $d_H = 6$ Å. For the slowest diffusion rates (corresponding to $d_H = 60$ Å), the solution will become supersaturated about 50 cm into the test section. This suggests that nucleation is possible within the range of model parameters, but if so, the salt deposit should have been spread over a greater length than observed in our experiments.

Considering the numerous modeling complexities, the predicted peak height is remarkably close to the measured peak height, regardless of flow rate or feed concentration.

Conclusions

Solubility of salts in supercritical water may be measured in a heated, flowing system provided that due consideration

is given to temperature profiles across the flow. This method has been used here for sodium sulfate in water at 25 MPa, providing new measurements at supercritical temperatures and confirmation of previous subcritical measurements.

The coupling between heat transfer, mass transfer, and solubility is important in the deposition of salts in a heated flow. These effects are considered in the model developed here; this model predicts peak salt layer thickness to within a factor of two of experimentally determined values, using salt hydrodynamic diameters of 2 to 6 Å. If ''critical slowing'' or Soret effects were significant in our experiments, the apparent hydrodynamic diameter would have been larger, but model runs with 60 Å diameters are not consistent with the measured salt distribution. Particle nucleation appears to be unimportant in our experiments.

Deposition modeling is hindered by the lack of information on the properties of solutions and turbulent mass transfer in supercritical fluids. This issue will become more important for mixtures actually encountered in supercritical water oxidation. For such mixtures, simple experimental techniques, such as those developed here, will have greater importance.

Acknowledgments

This work was made possible by funding from the British Columbia Science Council and NORAM Engineers and Constructors, Ltd.

Literature Cited

Armellini, F. J., and J. W. Tester, ''Solubility of Sodium Chloride and Sulfate in Sub- and Supercritical Water Vapor from 450–550°C and 100–250 bar,'' *Fluid Phase Equilib.*, **84**, 123 (1993).

Armellini, F. J., ''Phase Equilibria and Precipitation Phenomena of Sodium Chloride and Sodium Sulfate in Sub- and Supercritical Water,'' PhD Thesis, Dept. of Chemical Engineering, Mass. Inst. Technol., (1993).

Buelow, S. J., R. B. Dyer, D. M. Harradine, J. M. Robinson, R. C. Oldenborg, K. A. Funk, R. E. McInroy, J. A. Sanchez, and T. Spontarelli, ''Destruction of Energetic Materials by Supercritical Water Oxidation,'' Los Alamos report, LA-UR-93-3229 (1993).

Butenhoff, T. J., M. G. E. Goemans, and S. J. Buelow, ''Mass Diffusion Coefficients and Thermal Diffusivity in Concentrated Hydrothermal $NaNO_3$ Solutions,'' *J. Phys. Chem.*, **100**, 5982 (1996).

Chan, J. P. C., C. A. LaJeunesse, and S. F. Rice, ''Experimental Techniques to Determine Salt Formation and Deposition in Supercritical Water Oxidation Reactors,'' *HTD-Vol. 296, Fire, Combustion, and Hazardous Waste Processing*, S. Acharya, K. Annamalai, C. Presser, and R. D. Skocypec, eds., ASME, p. 171 (1994).

Cooper, S. P., H. G. Folster, S. A. Gairns, and E. G. Hauptmann, ''Treatment of Lagoon Sludge, Clarifier Sludge and Bleach Plant Effluent by Supercritical Water Oxidation,'' *Pulp and Paper Canada*, **98**, 37 (1997).

DiPippo, M. M., ''Phase Behavior of Inorganic Salts in Sub- and Supercritical Water,'' PhD Thesis, Dept. Chem. Eng., Mass Inst. of Technology, (1998).

Franck, E. U., ''Gas-Liquid and Gas-Solid Equilibria at High Pressure, Critical Curves and Miscibility Gaps,'' *Physical Chemistry: An Advanced Treatise*, Vol. 1, W. Jost, ed., Academic Press, New York, p. 367 (1971).

Gloyna, E. F., and L. Lixiang, ''Supercritical Water Oxidation Research and Development Update,'' *Env. Prog.*, **14**, 182 (1995).

Goldacker, H., J. Abeln, M. Kluth, A. Kruse, H. Schmieder, and G. Wiegand, ''Oxidation of Organic Material in Supercritical Water and Carbon Dioxide,'' *3rd. Int. Symp. on High Pressure Chemical Engineering*, Zurich, (1996).

Haar, L., J. S. Gallagher, and G. S. Kell, *NBS/NRC Steam Tables*, Hemisphere, Washington, DC (1984).

Hodes, M. S., K. A. Smith, W. S. Hurst, W. J. Bowers, and P. Griffith, ''Measurements and Modeling of Deposition Rates from a Near Supercritical Aqueous Sodium Sulfate Solution to a Heated Cylinder,'' HTD-Vol. 350, ASME Heat Transfer Conf., Baltimore, MD (1997).

Hodes, M. S., ''Measurements and Modeling of Deposition Rates from Near-Supercritical, Aqueous, Sodium Sulfate and Potassium Sulfate Solutions to a Heated Cylinder,'' PhD Thesis, Dept. of Mechanical Engineering, Mass. Inst. of Technology, (1998).

Hutchenson, K. W., and N. R. Foster, eds., *Innovations in Supercritical Fluids: Science and Technology*, Amer. Chem. Soc. (1995).

LaJuenesse, C. A., and S. F. Rice, ''Corrosion and Salt Deposition Issues in a Supercritical Water Oxidation Reactor,'' Sandia National Laboratories Report, 94-8468, Livermore, CA (1994).

Martynova, O. I., ''Solubility of Inorganic Compounds in Subcritical and Supercritical Water,'' *High Temperature and High Pressure Electrochemistry in Aqueous Solutions*, D. edG. Jones and R. W. Staehle, eds., Nat. Assoc. of Corrosion Engrs. (1976).

Martynova, O. I., and Y. F. Samoilov, ''The Formation of Solutions of Inorganic Substances in Water Vapor,'' *Russ. J. Inorg. Chem.*, **7**, 372 (1962).

McBrayer, R. N., and J. W. Griffith, ''Turn off the Heat,'' *Ind. Wastewater*, July, 43 (July–Aug. 1996).

Morey, G. W., and J. M. Hesselgesser, ''The Solubility of Some Minerals in Superheated Steam at High Pressures,'' *Econ. Geol.*, **46**, 821 (1951).

Oh, C. H., R. J. Kochan, and J. M. Beller, ''Numerical Analysis and Data Comparison of a Supercritical Water Oxidation Reactor,'' *AIChE J.*, **43**, 1627 (1997).

Protopopov, V. S., I. V. Kuraeva, E. V. Gorbacheva, T. E. Zav'yalova, M. V. Makaraov, and N. I. Fokina, ''Convective Diffusion of Iron-Corrosion Products in an Aqueous Coolant,'' *Thermal Eng.*, **41**, 170 (1994).

Pruss, A., and W. Wagner, ''A New Equation of State for Water as a Candidate of the New Scientific Formulation of IAPWS,'' *Physical Chemistry of Aqueous Systems: Meeting the Needs of Industry: Proc. Int. Conf. on Properties of Water and Steam*, H. J. White, J. V. Sengers, D. B. Newmann, and J. C. Bellows, eds, Begell House, New York, p. 66 (1995).

Ravich, M. L., and F. E. Borovaya, ''Phase Equilibria in the Sodium Sulphate-Water System at High Temperatures and Pressures,'' *Russ. J. Inorganic Chem.*, **9**, 520 (1964).

Rice, S. F., C. A. LaJeunesse, R. G. Hanush, J. D. Aitken, and S. C. Johnston, ''Supercritical Water Oxidation of Colored Smoke, Dye and Pyrotechnic Compositions: Phase I Final Report,'' Sandia National Laboratories Report, SAND94-8209, Livermore, CA (1994).

Shvedov, D., and P. R. Tremaine, ''The Solubility of Aqueous Sodium Sulfate and The Reduction of Sulfate by Magnetite under Near-Critical Conditions,'' *Proc. Int. Sym. on Hydrothermal Reactions*, D. A. Palmer and D. J. Wesolowski, eds., p. 1 (1997).

Shaw, R. W., T. B. Brill, A. A. Clifford, C. A. Eckert, and E. U. Franck, ''Supercritical Water Oxidation: A Medium for Chemistry,'' *C&E News*, 26 (Dec. 1991).

Swenson, H. S., J. R. Carver, and C. R. Kakarala, ''Heat Transfer to Supercritical Water in Smooth-Bore Tubes,'' *J. Heat Transfer*, 477 (Nov. 1965).

Tester, J. W., H. R. Holgate, F. J. Armellini, P. A. Webley, W. R. Killilea, G. T. Hong, and H. E. Barner, ''Supercritical Water Oxidation Technology: Process Development and Fundamental Research,'' *Emerging Technologies in Hazardous Waste Management*, D. W. Tedder and F. G. Pohland, eds., ACS Symp. Ser. 518, p. 35 (1993).

White, H. J., J. V. Sengers, D. B. Newmann, and J. C. Bellows, eds., *Physical Chemistry of Aqueous Systems: Meeting the Needs of Industry: Proceedings of the 12th International Conference on the Properties of Water and Steam*, Begell House, New York (1995).

Manuscript received July, 14, 1998, and revision received Nov. 30, 1998.